J. Phys. B: At. Mol. Opt. Phys. **41** (2008) 095402 (8pp) doi:10.1088/0953-4075/41/9/095402

Two-dimensional phase-space analysis and bifurcation study of the dynamical behaviour of a semiconductor ring laser

G Van der Sande[1,2], L Gelens[2], P Tassin[2], A Scirè[1] and J Danckaert[2]

[1] Instituto de Física Interdisciplinar y Sistemas Complejos (IFISC, CSIC-UIB), Campus Universitat Illes Balears, E-07122 Palma de Mallorca, Spain
[2] Department of Applied Physics and Photonics, Vrije Universiteit Brussel, Pleinlaan 2, 1050 Brussels, Belgium

E-mail: guy.van.der.sande@vub.ac.be

Received 4 December 2007, in final form 17 March 2008
Published 22 April 2008
Online at stacks.iop.org/JPhysB/41/095402

Abstract
A basic rate equation model of a quantum-well semiconductor ring laser is reduced to two equations using asymptotic methods. The reduced model allows for analytical expressions of the bifurcation points, which will simplify future model parameter estimations, and motivates a two-dimensional phase-space description of the dynamical behaviour. An analysis of the bifurcation scenarios in different parameter regimes is pursued. Physical conditions for the emergence of the operating regimes are assessed quantitatively in terms of saturation processes and backscattering mechanisms.

1. Introduction

Semiconductor ring lasers (SRLs) are promising candidates as key components in photonic integrated circuits. They do not require cleaved facets or gratings for optical feedback and are thus particularly suited for monolithic integration [1]. Because of their wavelength stability, they are highly desirable for applications such as wavelength filtering, unidirectional travelling-wave operation and multiplexing/demultiplexing applications [2–7]. Some monolithic SRLs exhibit a bistable unidirectional operation, which opens the possibility of using SRLs in systems for all-optical switching, gating, wavelength-conversion functions and optical memories [4, 8].

The problem of the directional operation of ring lasers has received a lot of interest since their first conception [9]. Different theoretical models focusing on the interplay between two counter-propagating modes and their interaction with the active medium have been proposed for the analysis of generalized rings and two-mode laser systems. Exploitation of the rotation-induced asymmetry between the two counter-propagating modes made ring lasers excellent candidates for gyroscopic systems. Because of this, the most widely studied systems are the He–Ne ring laser [10] and the CO_2 laser [11].

Driven by experimental results on CO_2 lasers, the theory of homogeneously and inhomogenously broadened solid-state ring lasers has been revisited in the 1980s. For a comprehensive overview, we refer to the work of Zeghlache *et al* [11] and references therein. In these investigations, the interaction between the two counter-propagating modes has been derived from first principles and is attributed to scattering on a spatial grating in the population inversion formed by the interference of both modes. A model for a homogeneously broadened ring laser taking the dynamics of this spatial grating into account shows rich dynamics ranging from stable unidirectional operation to complex chaotic dynamics depending on such parameters as the detuning [11–13]. The influence of the inhomogenous broadening on the stability boundaries has also been assessed [11, 14].

In the case of two-mode semiconductor lasers, it has been shown that phase-sensitive interactions between the modes are essential for the dynamical behaviour of the system. Etrich *et al* have proposed a model based on the time evolution of the electric fields [15]. They have addressed the effect of the slowly-varying carrier-induced grating originating from the interference of the two counter-propagating modes on the device operation. This leads to a nonlinear backscattering between the modes similar as in a solid-state ring laser. Other works highlight the emergence of intensity oscillations induced by mode to mode phase-coupling, such as Neelen *et al* [16], Mandel *et al* [17] and Khandokin *et al* [18].

A particular treatment for SRLs was devised by Sargent, who derived a simple model for the intensities of the two modes starting from first principles [19]. This work has pointed out the relevance of self- and cross-gain saturation processes in the dynamical operation of the device. Specifically, Sargent found that SRLs operate preferably unidirectionally due to gain saturation.

More recently, a comparison between experimental results in SRLs and a suitable theoretical explanation has been presented in [2, 3] by Sorel *et al*. They have experimentally observed bidirectional and unidirectional regimes of continuous-wave mode operation. Moreover, a bidirectional regime where the two counter-propagating modes experience harmonic alternate oscillations has been discovered. The theoretical framework used in [2, 3] is based on two mean-field equations for the counter-propagating modes, and a third rate equation for the carriers. The model accounts for self- and cross-gain saturation effects as in the work of Sargent [19] and includes backscattering contributions originating at the coupling to an output waveguide and has been found to be useful to study optical switching [20].

In this paper, we apply a singular perturbation technique to reduce the original laser equations to two equations. The analysis takes advantage of the different time scales present in the system. More specifically, the asymptotic analysis is valid on time scales slower than the relaxation oscillations. Not only do these reduced equations considerably simplify the bifurcation analysis of the possible steady-state solutions, they also allow for a two-dimensional phase-space description of the transitions between steady and time-periodic states.

This paper is organized as follows. In section 2, we formulate the model presented in [2, 3] and review the bifurcation analysis. This will be used as a guideline for our asymptotic analysis presented in section 3. The resulting reduced model equations are then studied in sections 4 and 5. We briefly study transient and switching phenomena in the reduced model (section 6). We conclude in section 7.

2. Formulation and primary bifurcations

The rate equation model for a SRL operating in a single longitudinal and single transversal modes can be derived from Maxwell–Bloch equations after adiabatic elimination of the material polarization dynamics [21]. The model presented in [2, 3] is therefore valid on time scales slower than the polarization decay rate and considers an electric field as the sum of the two counter-propagating waves:

$$E(z,t) = E_1(t)\exp[\mathrm{i}(\omega_0 t - k_0 z)] + E_2(t)\exp[\mathrm{i}(\omega_0 t + k_0 z)] + \mathrm{cc} \tag{1}$$

and is formulated mathematically in terms of two rate equations for the mean field slowly varying amplitudes $E_{1,2}$ of forward and backward propagating waves and one rate equation for the carrier number N. Neglecting transversal and longitudinal effects, the equations read [2, 3]:

$$\dot{E}_1 = \kappa(1+\mathrm{i}\alpha)[N(1 - s|E_1|^2 - c|E_2|^2) - 1]E_1 - (k_\mathrm{d} + \mathrm{i}k_\mathrm{c})E_2, \tag{2}$$

$$\dot{E}_2 = \kappa(1+\mathrm{i}\alpha)[N(1 - s|E_2|^2 - c|E_1|^2) - 1]E_2 - (k_\mathrm{d} + \mathrm{i}k_\mathrm{c})E_1, \tag{3}$$

$$\dot{N} = \gamma[\mu - N - N(1 - s|E_1|^2 - c|E_2|^2)|E_1|^2 - N(1 - s|E_2|^2 - c|E_1|^2)|E_2|^2], \tag{4}$$

where dot represents differentiation with respect to t. In equations (2)–(4), κ is the field decay rate, and γ is the decay rate of the carrier population. α is the linewidth enhancement factor and μ is the renormalized injection current ($\mu \approx 0$ at transparency, $\mu \approx 1$ at lasing threshold). The two-counter propagating modes interact both in a linear and nonlinear fashion [22]. They saturate both their own and each others gains through spectral hole burning and carrier heating effects. As the dynamics of these nonlinear processes occur on faster time scales than the photon lifetime of the SRL [23], these self- and cross-saturation effects can be added phenomenologically and are modelled by s and c. In contrast to the case of solid-state lasers [11], in the devices under study, the standing-wave pattern has a spatial period much smaller than the carrier diffusion length. Therefore, longitudinal variations of the carrier density will be washed out by the diffusion. As a result, the effects of such carrier grating on the dynamics can be neglected [3, 15, 18]. However, a linear phase coupling between the two-counterpropagating modes exists. Reflection of the counterpropagating modes can be caused by index variations within the ring cavity, at the interface between the circular cavity and the straight coupling waveguide and at the end facets of the output waveguides. These reflections result in a linear coupling between the two fields via the dissipative (k_d) and conservative (k_c) backscattering parameters [22, 24, 25].

Introducing the amplitude/phase decomposition

$$E_{1,2} = Q_{1,2}\,\mathrm{e}^{\mathrm{i}\phi_{1,2}}, \tag{5}$$

it is possible to rewrite equations (2)–(4)

$$\dot{Q}_1 = \kappa\left[N\left(1 - sQ_1^2 - cQ_2^2\right) - 1\right]Q_1 - k_\mathrm{d}Q_2\cos\psi + k_\mathrm{c}Q_2\sin\psi, \tag{6}$$

$$\dot{Q}_2 = \kappa\left[N\left(1 - sQ_2^2 - cQ_1^2\right) - 1\right]Q_2 - k_\mathrm{d}Q_1\cos\psi - k_\mathrm{c}Q_1\sin\psi, \tag{7}$$

$$\dot{\psi} = \kappa\alpha N(c-s)\left(Q_2^2 - Q_1^2\right) + k_\mathrm{d}\sin\psi\left(\frac{Q_2}{Q_1} + \frac{Q_1}{Q_2}\right) + k_\mathrm{c}\cos\psi\left(\frac{Q_2}{Q_1} - \frac{Q_1}{Q_2}\right), \tag{8}$$

$$\dot{N} = \gamma\left[\mu - N - N\left(1 - sQ_1^2 - cQ_2^2\right)Q_1^2 - N\left(1 - sQ_2^2 - cQ_1^2\right)Q_2^2\right], \tag{9}$$

where the relative phase ψ is defined by

$$\psi = \phi_2 - \phi_1. \tag{10}$$

Performing a numerical bifurcation analysis, the following scheme can be found (see figure 1). At the threshold current, $\mu \approx 1$, laser action starts. Although the counter-propagating modes experience strong nonlinear gain saturation, the

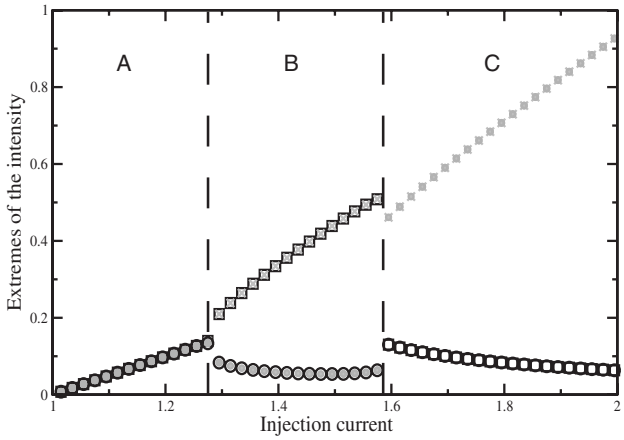

Figure 1. Bifurcation diagram of equations (2)–(4) depicting the extremes of the modal intensity versus injection current μ. Three regimes of operation are distinguished: (A) bidirectional CW operation, (B) alternate oscillations, (C) bistable unidirectional operation. $\kappa = 100\ \mathrm{ns}^{-1}$, $\gamma = 0.2\ \mathrm{ns}^{-1}$, $\alpha = 3.5$, $s = 0.005$, $c = 0.01\,k_\mathrm{d} = 0.0327\ \mathrm{ns}^{-1}$, $k_\mathrm{c} = 0.44\ \mathrm{ns}^{-1}$. The maxima (minima) of Q_1^2 are denoted by open black squares (circles). The maxima (minima) of Q_2^2 are denoted by grey crosses (dots).

dissipative backscattering k_d favours bidirectional emission (regime A in figure 1) just above threshold. The bidirectional regime corresponds to two symmetric solutions ($Q_1 = Q_2 = Q_0$ and $N = N_0$) with [2]

$$Q_0^2 = \frac{N_0 - 1 - k_\mathrm{d}\cos\psi}{(c+s)N_0}, \tag{11}$$

$$N_0 = \frac{\mu}{1 + 2Q_0^2 - 2(c+s)Q_0^4}. \tag{12}$$

These two solutions differ in their relative phase difference ψ. One of them has $\psi = 0$ and is referred to as the *in-phase symmetric solution* (IPSS), while the *out-of-phase symmetric solution* (OPSS) is characterized by $\psi = \pi$. Here, in regime A, due to the positive value of k_d, the OPSS is found to be the stable solution, while the IPSS is unstable. For the parameter set given in figure 1, the IPSS is of no further importance and all further bifurcations emerge from the OPSS.

Regime B is characterized by alternate intensity oscillations between the two counter-propagating modes. At $\mu \approx 1.3$, the OPSS loses its stability through a Hopf bifurcation point when [2]

$$4k_\mathrm{d} = \kappa N_0 Q_0^2 (c - s), \tag{13}$$

with Hopf frequency

$$\omega_\mathrm{H} = 2\sqrt{k_\mathrm{c}^2 - k_\mathrm{d}^2 - 2\alpha k_\mathrm{d} k_\mathrm{c}}. \tag{14}$$

At this point, a limit cycle representing a dynamic competition between the two counter-propagating modes appears. From equations (13) and (14), it is clear that this regime is due to the interplay between backscattering and saturation effects.

For injection currents larger than $\mu \approx 1.6$, in regime C, the optical output power is mainly concentrated in one propagation direction. This regime corresponds to two unstable out-of-phase asymmetric solutions (OPAS) emerging from a pitchfork bifurcation of the unstable OPSS. Because of the device symmetry two OPAS exist: one where $Q_1 > Q_2$ and vice versa. In this regime, the device exhibits bistability.

This succession of different dynamical regimes has been observed experimentally and the numerical modelling achieves a good qualitative and quantitative agreement with these experimental results [2, 3].

The above analysis has been performed numerically. The bidirectional regime and its corresponding Hopf point can be found by solving equations (11)–(13). However, the unidirectional regime can only be found by solving equations (6)–(9) numerically for its steady-state values using a Newton–Raphson method. This complicates the analysis of its bifurcation points, making a physical interpretation of the bifurcation schemes not straightforward. In the following section, we will show that it is possible to simplify the dynamical equations such that analytical results can be obtained for the unidirectional regime. Also, this analysis provides easier expressions for the bidirectional regime, eliminating the need for solving equations (11)–(13).

3. Analysis

Our numerical investigations of equations (2)–(4) show that the quantity $N - 1$ remains small on dynamical time scales longer than the relaxation oscillation period. This behaviour, which is quite generally observed in class B lasers [26], originates from the large ratio of carrier to photon lifetimes. Our simulations further show that this behaviour remains as long as the saturation coefficients s and c are of the same order or smaller than this ratio, while the backscatter parameters are smaller than the photon decay rate κ. It has been demonstrated in several experiments that such parameter values correspond to experimentally observed dynamics of SRLs [2, 3]. These parameter values suggest to investigate the limit

$$\kappa/\gamma \to \infty \tag{15}$$

assuming $N - 1, s$ and c smaller than 1, and k_d and k_c smaller than κ. The approach that we will follow here has already proven itself very successful in understanding the dynamical behaviour of other semiconductor laser devices, such as VCSELs [27, 28].

To be able to define the order of magnitude of all parameters and determine the leading order approximation to equations (6)–(9), we need to introduce a dimensionless time

$$\tau = \gamma t, \tag{16}$$

and a smallness parameter ρ as

$$\rho = \frac{\gamma}{\kappa}. \tag{17}$$

From numerical simulations, we have seen that N always evolves close to the threshold value. Hence, we define a new carrier variable

$$N - 1 = \rho n \tag{18}$$

where n is assumed to be $O(1)$. Note that in this analysis, the carrier number N is assumed close to its steady-state value, whereas the field variables are allowed to evolve arbitrarily. We further assume that

$$s = \rho S, \tag{19}$$

$$c = \rho C, \tag{20}$$

$$k_\mathrm{d}/\kappa = \rho K_\mathrm{d}, \tag{21}$$

$$k_\mathrm{c}/\kappa = \rho K_\mathrm{c}, \tag{22}$$

with S, C, K_d and K_c of $O(1)$. After substituting equations (16)–(22) into equations (6)–(9) and taking the limit $\rho \to 0$, we obtain the following leading order system:

$$Q_1' = \left(n - SQ_1^2 - CQ_2^2\right)Q_1 - K_\mathrm{d}Q_2\cos\psi + K_\mathrm{c}Q_2\sin\psi, \tag{23}$$

$$Q_2' = \left(n - SQ_2^2 - CQ_1^2\right)Q_2 - K_\mathrm{d}Q_1\cos\psi - K_\mathrm{c}Q_1\sin\psi, \tag{24}$$

$$\psi' = \alpha(C-S)\left(Q_2^2 - Q_1^2\right) + K_\mathrm{d}\sin\psi\left(\frac{Q_2}{Q_1} + \frac{Q_1}{Q_2}\right) + K_\mathrm{c}\cos\psi\left(\frac{Q_2}{Q_1} - \frac{Q_1}{Q_2}\right), \tag{25}$$

$$1 - \mu + Q_1^2 + Q_2^2 = 0, \tag{26}$$

where prime now denotes derivation with respect to the dimensionless time τ. The first three equations (23)–(25) are a simplified form of the original rate equations (6)–(8). However, equation (26) is not a rate equation and does not give us an expression for n. At this point, it is clear that our analysis differs considerably from an adiabatic elimination of the carrier dynamics. Instead, we have derived a conservation law for the total intensity $Q_1^2 + Q_2^2$ given by

$$Q_1^2 + Q_2^2 = \mu - 1 > 0. \tag{27}$$

This conservation law is valid on the slow time scale τ. Practically, this means that when reaching the conservation relation dynamically (e.g. after a step in the injected current) the typical relaxation oscillations are observed on a faster timescale with typical frequency $\sim \sqrt{(\mu-1)/\rho}$. On the slow timescale, however, this transition will seem to have appeared abruptly. So, on the slow time τ the total power will remain conserved. As a result, the carrier number n will become a slaved variable. We can now use this property to determine n from the equations for the amplitudes $Q_{1,2}$. Combining equations (23) and (24), we can find

$$\left(Q_1^2 + Q_2^2\right)' = 2n\left(Q_1^2 + Q_2^2\right) - 2S\left(Q_1^4 + Q_2^4\right) - 4CQ_1^2Q_2^2 - 4K_\mathrm{d}Q_1Q_2\cos\psi = 0. \tag{28}$$

Because of the conservation law in equation (27), equation (28) reduces to an algebraic equation relating n to Q_1, Q_2 and ψ. Also, $Q_2(Q_1) = \sqrt{\mu - 1 - Q_1^2}$. We find

$$n(Q_1,\psi) = \frac{1}{\mu-1}\left\{S\left[Q_1^4 + Q_2^4(Q_1)\right] + 2CQ_1^2Q_2^2(Q_1) + 2K_\mathrm{d}Q_1Q_2(Q_1)\cos\psi\right\}. \tag{29}$$

Substituting equation (29) into equations (23)–(25), we finally get a closed set of two rate equations

$$Q_1' = \left[n(Q_1,\psi) - SQ_1^2 - CQ_2^2(Q_1)\right]Q_1 - K_\mathrm{d}Q_2(Q_1)\cos\psi + K_\mathrm{c}Q_2(Q_1)\sin\psi, \tag{30}$$

$$\psi' = \alpha(C-S)\left[Q_2^2(Q_1) - Q_1^2\right] + K_\mathrm{d}\sin\psi\left[\frac{Q_2(Q_1)}{Q_1} + \frac{Q_1}{Q_2(Q_1)}\right] + K_\mathrm{c}\cos\psi\left[\frac{Q_2(Q_1)}{Q_1} - \frac{Q_1}{Q_2(Q_1)}\right]. \tag{31}$$

These two coupled rate equations represent the leading order approximation to the original four equations.

Using the conservation law of equation (27) for one last time, equations (30), (31) can be rewritten in a more appealing form. We define the dynamical variable θ as a measure for the relative modal intensity by

$$Q_1 = \sqrt{\mu - 1}\cos\left(\frac{\theta + \pi/2}{2}\right), \tag{32}$$

$$Q_2 = \sqrt{\mu - 1}\sin\left(\frac{\theta + \pi/2}{2}\right), \tag{33}$$

with $\theta \in [-\pi/2, \pi/2]$. Defining $J = (C-S)(\mu-1)$, the reduced equations now read

$$\theta' = -2K_\mathrm{c}\sin\psi + 2K_\mathrm{d}\cos\psi\sin\theta + J\sin\theta\cos\theta, \tag{34}$$

$$\cos\theta\,\psi' = \alpha J\sin\theta\cos\theta + 2K_\mathrm{d}\sin\psi + 2K_\mathrm{c}\cos\psi\sin\theta. \tag{35}$$

Note that the renormalized injection current J can be either positive or negative depending on the sign of $C - S$.

4. Special cases

In order to better understand the emerging dynamical behaviour of SRLs, we will study equations (34), (35) in two extreme cases. First, we consider that the nonlinear gain saturation processes balance each other ($C = S$). This results in zero renormalized current $J = 0$, and therefore any effect of injection current μ disappears. In this case, only the backscattering process influences the dynamics of the modes. Because backscattering constitutes a linear coupling between the fields, we will refer to this case as the linear coupling regime. In the second case, we assume that no linear backscattering is present ($K_\mathrm{d} = K_\mathrm{c} = 0$), so that the dynamics is determined only by the strength of J. We will refer to this case as the nonlinear coupling regime. Both regimes are actually unrealistic for SRLs. While saturation can be neutral ($C = S$) in He–Ne ring lasers [24], for a SRL the saturation processes are not expected to cancel, as due to spectral hole burning and carrier heating effects C is expected to be equal to $2S$ [22]. Backscattering is unavoidable in SRLs since the light in the ring needs to be coupled out via a coupler waveguide, that always implies small reflections. Nevertheless, the study of these special cases will ease our understanding of the dynamics of the general case.

4.1. The linear coupling

When $J = 0$, equations (34) and (35) reduce to

$$\theta' = -2K_c \sin\psi + 2K_d \cos\psi \sin\theta, \tag{36}$$
$$\cos\theta\psi' = 2K_d \sin\psi + 2K_c \cos\psi \sin\theta. \tag{37}$$

Solving equations (36) and (37) for their steady states, we find

$$\theta = 0 \qquad \text{and} \qquad \sin\psi = 0, \tag{38}$$

which corresponds to bidirectional emission. So, backscattering effects will thus force the SRL to emit in both directions. This is a good point to remark that these bidirectional solutions are independent from the injection current J. On the slow timescale τ, rapidly changing the current will therefore make the intensity of this solution jump infinitely fast (see equations (32) and (33)) and without relaxation oscillations. Of course, in the original model, such a switch would be accompanied by an initial fast transient of relaxation oscillations.

4.2. The nonlinear coupling

When $K_d = K_c = 0$, equations (34) and (35) reduce to

$$\theta' = J \sin\theta \cos\theta, \tag{39}$$
$$\cos\theta\psi' = \alpha J \sin\theta \cos\theta, \tag{40}$$

which also has bidirectional emission as a steady-state solution. A second steady-state solution,

$$\theta = \pm\frac{\pi}{2}, \tag{41}$$

corresponds to pure unidirectional emission. The sign of J will determine which of the two solutions is stable. For positive J, it will always be the unidirectional emitting one, whereas for negative J, the SRL would still be emitting in both directions. One can conclude that stronger cross-saturation than self-saturation ($C > S$) gives preference to unidirectional emission.

5. Linear stability analysis

In this section, we will perform the steady-state analysis of the reduced equation set (34) and (35) describing the slow time dynamics of SRLs. This will show us how the linear and nonlinear coupling compete. Thanks to the two-dimensionality of the given problem, the linear stability can be studied analytically. The bifurcation diagrams of the periodic solutions still need to be constructed numerically. Moreover, equations (34) and (35) motivate that the slow time dynamical behaviour of the system is limited to the phase plane (θ, ψ).

5.1. Bidirectional solutions

Equating equations (34) and (35) to zero, it is clear that the steady-state (bidirectional) symmetric solutions are given by

$$\theta = 0, \tag{42}$$
$$\sin\psi = 0, \tag{43}$$

with $\psi = 0$ for the IPSS and $\psi = \pi$ for the OPSS. Using equations (34) and (35), we can study the linear stability of these steady-state solutions. Considering small perturbations around the steady-state values, we find the following characteristic equation:

$$\lambda^2 - \lambda(J \pm 4K_d) \pm 2J(K_d + \alpha K_c) + 4\left(K_c^2 + K_d^2\right) = 0, \tag{44}$$

where the upper (lower) sign corresponds to the IPSS (OPSS). The IPSS is stable for

$$J < J^H_{IPSS} = -4K_d, \tag{45}$$

and

$$J > J^S_{IPSS} = -2\frac{K_c^2 + K_d^2}{K_d + \alpha K_c} \qquad \text{for} \quad K_d + \alpha K_c > 0, \tag{46}$$

$$J < J^S_{IPSS} = -2\frac{K_c^2 + K_d^2}{K_d + \alpha K_c} \qquad \text{for} \quad K_d + \alpha K_c < 0. \tag{47}$$

J^H_{IPSS} is a Hopf bifurcation point with frequency

$$\Omega^H_{IPSS} = 2\sqrt{K_c^2 - K_d^2 - 2K_c K_d \alpha}, \tag{48}$$

and J^S_{IPSS} a static bifurcation point. The OPSS is stable for

$$J < J^H_{OPSS} = 4K_d, \tag{49}$$

and

$$J < J^S_{OPSS} = 2\frac{K_c^2 + K_d^2}{K_d + \alpha K_c} \qquad \text{for} \quad K_d + \alpha K_c > 0, \tag{50}$$

$$J > J^S_{OPSS} = 2\frac{K_c^2 + K_d^2}{K_d + \alpha K_c} \qquad \text{for} \quad K_d + \alpha K_c < 0 \tag{51}$$

J^H_{OPSS} is a Hopf bifurcation point with frequency

$$\Omega^H_{OPSS} = 2\sqrt{K_c^2 - K_d^2 - 2K_c K_d \alpha} = \Omega^H_{IPSS}, \tag{52}$$

and J^S_{OPSS} a static bifurcation point.

5.2. Unidirectional solutions

The unidirectional asymmetric solutions are less straightforward to obtain. An elegant approach to writing an analytical expression for these solutions is to parametrize them in ψ. The solution is then of the form $\{\theta(\psi), J(\psi)\}$:

$$\theta_{AS}(\psi) = \arcsin\left(\frac{\alpha K_c + K_d}{\alpha K_d - K_c}\tan\psi\right), \tag{53}$$

$$J(\psi) = 2\csc\theta(\psi)\sec\theta(\psi)[K_c \sin\psi - K_d \cos\psi \sin\theta(\psi)]. \tag{54}$$

Four asymmetric solutions exist: two that originate at a pitchfork bifurcation from the IPSS ($\theta = 0, \psi = 0$), and two from the OPSS ($\theta = 0, \psi = \pi$). We will refer to them as IPAS and OPAS, respectively. Now also, the pitchfork bifurcation currents can be obtained analytically:

$$J^{PF}_{IPAS} = J^S_{IPSS} = -2\frac{K_c^2 + K_d^2}{K_d + \alpha K_c}, \tag{55}$$

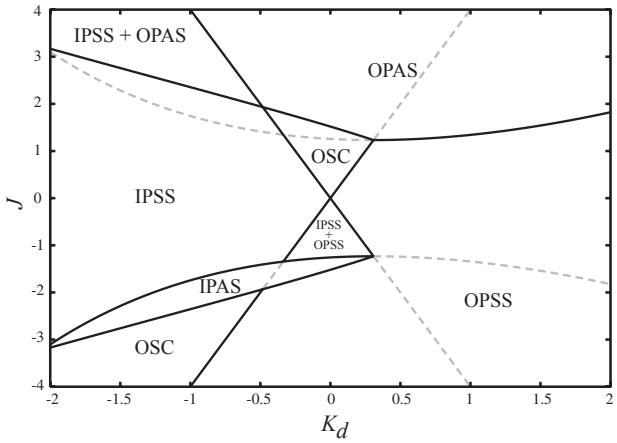

Figure 2. Stability diagram in the plane (K_d, J) for fixed values of $K_c = 2.2$ and $\alpha = 3.5$ showing the different stable operation regimes. The lines indicate the bifurcation currents as derived in sections 5.1 and 5.2. Black solid lines denote transitions between stable operating regimes, whereas dashed grey lines are bifurcation lines that do not alter the stability of the operating regimes.

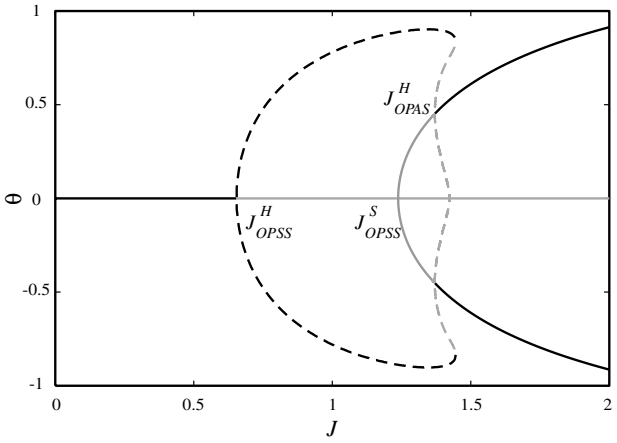

Figure 3. Bifurcation diagram of equations (34) and (35) depicting the extremes of θ versus injection current J. The steady-state values of θ are denoted by full lines, while the extrema of periodically oscillating θ are indicated with dashed lines. Black colour is used for stable fixed points or limit cycles, and grey for unstable fixed points or limit cycles. $K_d = 0.1635$, $\alpha = 3.5$.

$$J^{PF}_{OPAS} = J^S_{OPSS} = 2\frac{K_c^2 + K_d^2}{K_d + \alpha K_c}. \tag{56}$$

These solutions are destabilized at a Hopf bifurcation point

$$\tan^2 \psi^H_{AS} = \frac{(K_c - K_d\alpha)^2\left(K_c^2 - K_d^2 - 2K_cK_d\alpha\right)}{(K_d + K_c\alpha)^2\left(3K_c^2 + K_d^2 - 2K_cK_d\alpha\right)} \tag{57}$$

with the IPAS stable for

$$\tan^2 \psi < \tan^2 \psi^H_{AS} \tag{58}$$

and the OPAS stable for

$$\tan^2 \psi > \tan^2 \psi^H_{AS}. \tag{59}$$

5.3. Stability diagram

In figure 2, we have summarized the previous results. We have plotted the analytically obtained bifurcation currents as a function of the dissipative backscattering parameter K_d for a fixed value of the conservative backscattering parameter $K_c = 2.2$ and linewidth enhancement factor $\alpha = 3.5$. We study both positive and negative current values J corresponding to $C > S$ and $C < S$. The bifurcation currents distinguish between no less than seven different operating regimes in this parameter range: IPSS, OPSS, bistable OPAS, bistable IPAS, oscillatory behaviour (OSC), tristability between the IPSS and the two OPAS (IPSS + OPAS), bistability between IPSS and OPSS (IPSS + OPSS). Note that depending on the type of Hopf bifurcation (super- or subcritical), narrow regions of oscillations can be expected around the Hopf bifurcation lines. To gain insight in the mechanisms leading to the appearance of these dynamical regimes, we will now consider two current paths at different K_d which are representatives of different bifurcation scenarios.

At $K_d = 0.1635$, we construct the bifurcation diagram of θ with J as the bifurcation parameter (see figure 3). Note

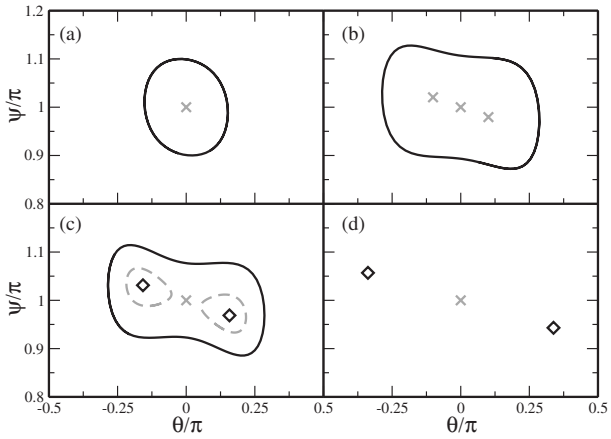

Figure 4. Phase-space structure at $K_d = 0.1635$ and $\alpha = 3.5$ for different values of the injection current J. (a) $J = 0.75$, (b) $J = 1.3$, (c) $J = 1.4$, (d) $J = 2.0$. Black diamonds indicate stable fixed points. Unstable fixed points are denoted by grey crosses. Black solid lines are used for stable limit cycles and grey dashed lines for unstable limit cycles.

that this corresponds to the original parameters as in figure 1. For this value of K_d, we restrict ourselves to positive values of J. The two-dimensional phase-space structure in figure 4 illustrates the dynamical behaviour in the different operating regimes. At $J = 0$, the OPSS is selected. When increasing the current, the OPSS is destabilized at the Hopf bifurcation point J^H_{OPSS}. At this Hopf point, a stable limit cycle centred around the OPSS emerges (figure 4(a)). The amplitude of these time-periodic oscillations continues to grow with J. At the pitchfork bifurcation J^S_{OPSS}, two OPAS fixed points appear (figure 4(b)). These fixed points are unstable until the current exceeds the Hopf point J^H_{OPAS}. From this point, small unstable limit cycles grow from both OPAS (figure 4(c)). The stable limit cycle centred around the unstable OPSS, connects with

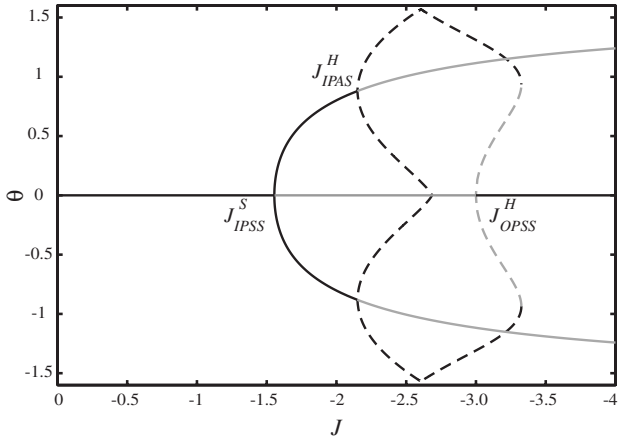

Figure 5. Bifurcation diagram of equations (34) and (35) depicting the extremes of θ versus injection current J. The steady-state values of θ are denoted by full lines, whereas the extrema of periodically oscillating θ are indicated with dashed lines. Black is used for stable fixed points or limit cycles, and grey for unstable fixed points or limit cycles. $K_d = -0.75$, $\alpha = 3.5$.

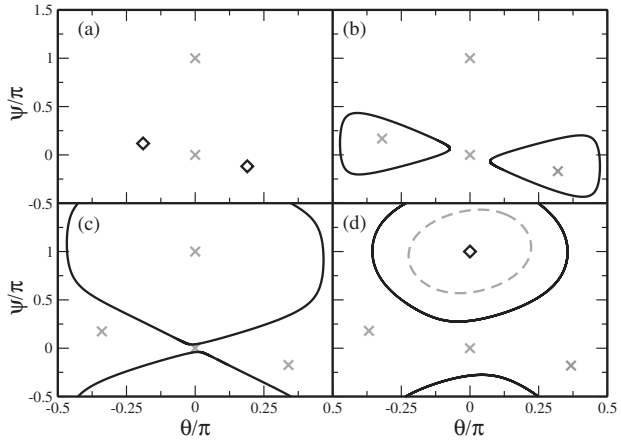

Figure 6. Phase-space structure at $K_d = -0.75$ and $\alpha = 3.5$ for different values of the injection current J. (a) $J = -1.75$, (b) $J = -2.5$, (c) $J = -2.75$, (d) $J = -3.25$. Black diamonds indicate stable fixed points. Unstable fixed points are denoted by grey crosses. Black solid lines are used for stable limit cycles and grey dashed lines for unstable limit cycles.

the unstable limit cycles centred around the OPAS, and these time-periodic structures disappear (figure 4(d)).

At $K_d = -0.75$, we show the bifurcation diagram of θ with J as the bifurcation parameter (see figure 5). For this value of K_d, we have restricted ourselves to negative values of J. At $J = 0$, the IPSS is selected. It loses its stability through a pitchfork bifurcation at J^S_{IPSS}, forming the two stable IPAS (figure 6(a)). The unidirectional IPAS solutions are both destabilized in a Hopf bifurcation at J^H_{IPAS}. In figure 6(b), one can see that beyond this point two stable limit cycles centred around the IPAS are formed. The amplitude of these oscillations grows until both limit cycles connect, creating a new limit cycle centred around the unstable OPSS (figure 6(c)). The OPSS becomes Hopf stable at J^H_{OPSS} with the emergence of

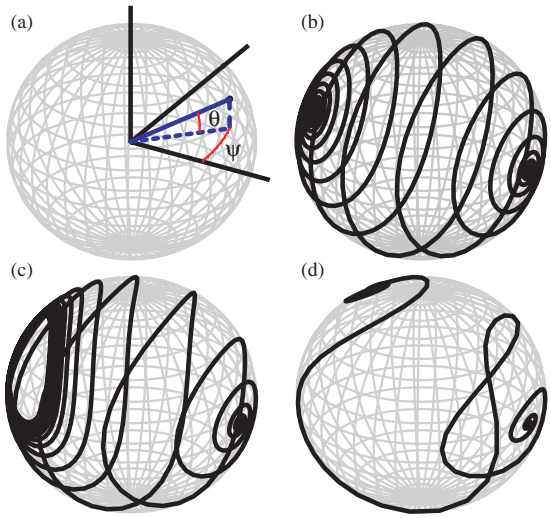

Figure 7. Examples of phase-space portraits in the spherical phase space for $K_d = 0.1635$ and $\alpha = 3.5$. The angles θ and ψ are defined as in (a). (b) Time evolution from the unstable IPSS to the stable OPSS ($J = 0.5$). (c) Time evolution from the unstable IPSS to the stable oscillations ($J = 0.75$). (d) Time evolution from the unstable IPSS to one of the stable OPAS ($J = 2.0$).

(This figure is in colour only in the electronic version)

an unstable limit cycle (figure 6(d)). This unstable limit cycle then collides with the larger stable one in a fold bifurcation. For higher currents, only the OPSS remains stable.

As a final point, we want to remark that a symmetry exists in the bifurcation points derived in sections 5.1 and 5.2. Changing the sign of both K_d and K_c will keep the position of the bifurcation points unchanged. However, the role of the in-phase solutions and out-of-phase solutions will have been exchanged. As a result, if $K_c = 0$, we can expect figure 2 to be symmetric in K_d. If the linewidth enhancement factor $\alpha = 0$, the stability diagram will show this symmetry for any K_c.

6. Spherical phase portraits

Because we have reduced the dynamics of the system to a phase space consisting of two angles θ and ψ, it is possible to study the properties of the solutions on a sphere. If the angles would be defined as the spherical coordinates (as in figure 7(a)), then bidirectional emission fixed points ($\theta = 0$) would be situated along the equator with the IPSS and the OPSS opposite to each other. Purely unidirectional emission ($\theta = \pm\pi/2$) can be found on the north ($\theta = +\pi/2$) and south pole ($\theta = -\pi/2$). We will use this representation to study the transient behaviour exhibited by the SRL. We focus on the bifurcation scheme as presented in figure 3 ($K_d = 0.1635$ and $\alpha = 3.5$). In this case, the IPSS is always unstable and we will use it as our initial condition. In figures 7(b)–(d), we let the system evolve from this point for different values of the injection current J. In figure 7(b), the current is fixed such that the only other attractor in the phase space is the stable OPSS. As is clear from this figure, the system spirals along the sphere in a specific way from the IPSS to the diametrically opposed OPSS. In

figure 7(c), a limit cycle is the stable attractor. This limit cycle clearly distorts the spiral. When the OPAS has become stable (figure 7(d)), the spiral disappears and the system snakes from the IPSS to one of the OPAS which is now close to the north pole.

7. Conclusion

In this paper, we have used asymptotic methods to derive a two-variable reduced model for the dynamical behaviour of semiconductor ring laser. The model accounts for both backscattering processes and gain saturation effects. The mathematical analysis is motivated by the relative magnitudes of experimentally reasonable parameters. Thanks to this analysis, we have been able to perform a systematic and largely analytical bifurcation study of all the steady states and time-periodic states of the model. Our analysis has shown that also other types of bifurcations—than previously studied and experimentally demonstrated in this system—might be expected depending on the parameter values. Of particular interest are Hopf bifurcation points to stable and unstable time-periodic regimes. Together with the bifurcation analysis, the two-dimensionality of the reduced model has eased the understanding of the appearance of the different operating regimes. Finally, studying the transient behaviour of the system on a sphere will help future physical interpretations of switching processes.

Acknowledgments

This work has been partially funded by the European Community under project IST-2005-34743 (IOLOS). This work was supported by the Belgian Science Policy Office under grant no. IAP-VI10. GV is a Postdoctoral Fellow and LG and PT are PhD Fellows of the Research Foundation—Flanders (FWO). AS acknowledges the Ramon y Cajal program by MEC. The authors are grateful to Toni Pérez for careful reading of the manuscript.

References

[1] Krauss T, Laybourn P J R and Roberts J S 1990 CW operation of semiconductor ring lasers *Electron. Lett.* **26** 2095–7
[2] Sorel M, Laybourn J P R, Sciré A, Balle S, Giuliani G, Miglierina R and Donati S 2002 Alternate oscillations in semiconductor ring lasers *Opt. Lett.* **27** 1992–4
[3] Sorel M, Giuliani G, Sciré A, Miglierina R, Laybourn J P R and Donati S 2003 Operating regimes of GaAs–AlGaAs semiconductor ring lasers: experiment and mode *IEEE J. Quantum Electron.* **39** 1187–95
[4] Liang J J, Lau S T, Leary M H and Ballantyne J M 1997 Unidirectional operation of waveguide diode ring lasers *Appl. Phys. Lett.* **70** 1192–4
[5] Zhang S, Liu Y, Lenstra D, Hill M T, Ju H, Khoe G D and Dorre H J S 2004 Ring-laser optical flip-flop memory with single active element *IEEE J. Sel. Top. Quantum Electron.* **10** 1093–100
[6] Almeida V R, Barrios C A, Panepucci R P, Lipson M, Foster M A, Ouzounov D G and Gaeta A L 2004 All-optical switching on a silicon chip *Opt. Lett.* **29** 2867–9
[7] Almeida V R and Lipson M 2004 Optical bistability on a silicon chip *Opt. Lett.* **29** 2387–9
[8] Hill M T, Dorren H J S, de Vries T, Leijtens X J M, den Besten J H, Smalbrugge B, Oei Y S, Binsma H, Khoe G D and Smit M K 2004 A fast low-power optical memory based on coupled micro-ring lasers *Nature* **432** 206–9
[9] Aronowitz F 1965 Theory of a traveling-wave optical maser *Phys. Rev.* **139** A635
[10] Menegozzi L N and Lamb W E 1973 Theory of a ring laser *Phys. Rev.* A **8** 2103–25
[11] Zeghlache H, Mandel P, Abraham N B, Hoffer L M, Lippi G L and Mello T 1988 Bidirectional ring laser: Stability analysis and time-dependent solutions *Phys. Rev.* A **37** 470–97
[12] Mandel P and Agrawal G P 1982 Mode instabilities in a homogenously broadened ring laser *Opt. Commun.* **42** 269–74
[13] Mandel P and Zeghlache H 1983 Stability of a detuned single mode homogenously broadened ring laser *Opt. Commun.* **47** 146–50
[14] Mandel P, Nardone P and Erneux T 1988 Periodic loss modulation in a ring laser—influence of inhomogenous broadening and detuning *J. Opt. Soc. Am.* B **5** 1113–20
[15] Etrich C, Mandel P, Abraham N B and Zeghlache H 1992 Dynamics of a two-mode semiconductor laser *IEEE J. Quantum Electron.* **28** 811–21
[16] Neelen R C, Van Exter M P, Bouwmeester D and Woerdman J P 1992 Mode competition in a semiconductor ring laser *J. Mod. Opt.* **39** 1623–41
[17] Mandel P, Etrich C and Otsuka K 1993 Laser rate equations with phase-sensitive interactions *IEEE J. Quantum Electron.* **29** 836–43
[18] Khandokhin P A, Koryukin I V, Khanin Ya I and Mandel P 1995 Influence of carrier diffusion on the dynamics of a two-mode laser *IEEE J. Quantum Electron.* **31** 647–52
[19] Sargent III M 1993 Theory of a multimode quasiequilibrium semiconductor laser *Phys. Rev.* A **48** 717–26
[20] Pérez T, Scirè A, Van der Sande G, Colet P and Mirasso C R 2007 Bistability and all-optical switching in semiconductor ring lasers *Opt. Express* **15** 12941–8
[21] Sargent III M, Scully M O and Lamb W E 1974 *Laser Physics* (Reading, MA: Addison-Wesley)
[22] Born C, Sorel M and Yu S 2005 Linear and nonlinear mode interactions in a semiconductor ring laser *IEEE J. Quantum Electron.* **41** 261–71
[23] Willatzeb M, Uskov A, Mørk J, Olesen H, Tromborg B and Jauho A-P 1991 Linear and nonlinear mode interactions in a semiconductor ring laser *IEEE Photon. Technol. Lett.* **3** 606–9
[24] Spreeuw R J C, Neelen R C, van Druten N J, Eliel E R and Woerdman J P 1990 Mode coupling in a He–Ne ring lasers with backscattering *Phys. Rev.* A **42** 4315–24
[25] Etrich C, Mandel P, Neelen R C, Spreeuw R J C and Woerdman J P 1992 Dynamics of a ring-laser gyroscope with backscattering *Phys. Rev.* A **46** 525–36
[26] Carr T W and Erneux T 1994 Hopf bifurcation of the class-B multimode laser *Phys. Rev.* A **50** 724–31
[27] Erneux T, Danckaert J, Panajotov K and Veretennicoff I 1999 Two-variable reduction of the San Miguel–Feng– Moloney model for vertical-cavity surface-emitting lasers *Phys. Rev.* A **59** 4660–7
[28] Van der Sande G, Danckaert J, Veretennicoff I and Erneux T 2003 Rate equations for vertical-cavity surface-emitting lasers *Phys. Rev.* A **67** 013809